Improper multiferroiclike transition in a metal

Zhigang Gui, Chao Gu, Hu Cheng, Jinlong Zhu, Xiaohui Yu, Er-jia Guo, Liusuo Wu, Jiawei Mei, Jieming Sheng, Jianzhong Zhang, Junling Wang, Yusheng Zhao, Laurent Bellaiche, Li Huang, and Shanmin Wang

Phys. Rev. B **105**, L180101 — Published 19 May 2022

DOI: 10.1103/PhysRevB.105.L180101

Improper multiferroic-like transition in a metal

Zhigang Gui,[1,§] Chao Gu,[1,§] Hu Cheng,[1] Jinlong Zhu,[1] Xiaohui Yu,[2] Er-jia Guo,[2] Liusuo Wu,[1] Jiawei Mei,[1] Jieming Sheng,[1] Jianzhong Zhang,[3] Junling Wang,[1] Yusheng Zhao[1], Laurent Bellaiche,[4] Li Huang,[1,*] and Shanmin Wang[1,*]

[1]*Department of Physics & Academy for Advanced Interdisciplinary Studies, Southern University of Science & Technology, Shenzhen, Guangdong, 518055, China*
[2]*Beijing National Laboratory for Condensed Matter Physics and Institute of Physics, Chinese Academy of Sciences, Beijing 100190, China*
[3]*Materials Science & Technology Division, Los Alamos National Laboratory, Los Alamos, NM 87545, USA*
[4]*Physics Department and Institute for Nanoscience and Engineering, University of Arkansas, Fayetteville, AR 72701, USA*

Abstract

Magnetic frustration in insulators often induces cooperative atomic displacements to form polar structure with long-range ordered electric dipoles, commonly known as improper multiferroics. In metals, such multiferroic phenomenon is not expected to occur because free carriers tend to screen internal electrostatic forces, eliminating long-range ordered electric dipoles. To date, intrinsic multiferroic-like metals have rarely been reported. Here we present a spin-frustration-induced long-range antiparallel ordering of electric dipoles in metallic CrN with an unusual antiferromagnetic ground state. Two equivalent magnetic structures are also identified and linked to two distinct antiparallel polar orders. Such a scenario is analogous to that of conventional improper multiferroics with a magnetic origin of polar transition. The order parameter of structural distortion is linearly coupled to the magnetic order, due to a strong magnetoelectric effect. The multiferroic-like metal is in striking contrast to insulating multiferroics, offering an extraordinary archetype for probing new underlying physics and exploring unusual properties for practical applications.

Keywords: *CrN, correlated-electron system, frustrated magnetism, polar transition*

Introduction

Multiferroics with intimately coupled magnetism and (anti)ferroelectricity are found in strongly correlated insulators [1-5], especially the 3d transition-metal oxides with localized 3d electrons that are a crucial ingredient for producing magnetism. Most of these materials often have a peculiar antiferromagnetic (AFM) ground state with involvement of a complex magnetic order and frustrated spin, which is key to inducing the long-range ordered electric dipoles for (anti)ferroelectricity [3,4]. However, in most metallic oxides, conductive electrons are closely related to the delocalized 3d electrons, which are mutually exclusive with AFM ordering where electron localization is required. On the other hand, free carriers in metals tend to eliminate the cooperative alignment of electric dipoles and eventually preclude the (anti)ferroelectricity [6-9]. Thus, it is exceedingly unusual to find an intrinsic polar metal with coexisting long-range magnetic order.

Possibility of coexisting contra-indicated properties of both polarity and metallicity in a material to form "ferroelectric" metal was predicted by Anderson and Blount in 1965[7]. In fact, such polar metals are not uncommon and was reported in a number of non-centrosymmetric materials [8,10], but none of them exhibit a nonpolar-to-polar transition under external fields. A recent surge of studies along this direction has led to the discovery of a few rare cases of polar transitions in metallic materials. A convincing example is metallic $LiOsO_3$, which exhibits a ferroelectric-like transition as a result of anisotropic displacement of Li ions [6,11,12]. An electrically or chemically switchable polarity was recently identified in atomically-thin layers of WTe_2 and 1T′-

$MoTe_2$, due to the electron-hole correlation effect [13,14]. In principle, the polar metals can be tuned by introducing a weak electron-lattice coupling [10]. Perovskite oxides (i.e., ABO_3), such as geometrically designed $NdNiO_3$ thin films [15], are in this regard the best candidates, where the B ions contribute partially-occupied delocalized states at the Fermi level for conduction, which are decoupled from electric polarization associated with the A ions. The driving force for polar displacement in thin-film $NdNiO_3$ is the local suppression of NiO_6 tilt angle by the substrate [15]. A weakly coupled electron mechanism was also revealed in $LiOsO_3$ [16], and a few polar metal candidates were recently reported in complex compounds [17-19]. However, those ferroelectric-like metals are either geometrically or electronically stabilized without involving magnetism. Possible multiferroic-like metals with undetectable polarity were recently studied (e.g., Pb_2CoOsO_6) [20,21]. By now, no other polar or antipolar metal has been found to have a magnetic origin.

Here we show that CrN is an intrinsic metal and undergoes an antiferroelectric (AFE)-like transition at low temperatures, driven by a frustrated AFM ordering that is associated with the localized Cr: t_{2g} electrons. The metallicity originates from the hybridization of Cr: e_g - N: p orbitals, which decouples from the soft phonons that are linked to the antiparallel ordering of electric dipoles. The phase transition and magnetoelectric effect are well explored and a ferrielectric (FERRI)-like metal CrN is predicted under epitaxial strain.

Results and Discussion

Because of experimental difficulties in preparing well-crystallized bulk sample, properties of CrN have not been well understood [22-28]. Based on high-pressure synthesized high-quality CrN [29,30], we performed low-temperature (T) neutron powder diffraction (NPD) measurement [31] (Fig. 1). Experimental details are described in the Supplemental Material[32].

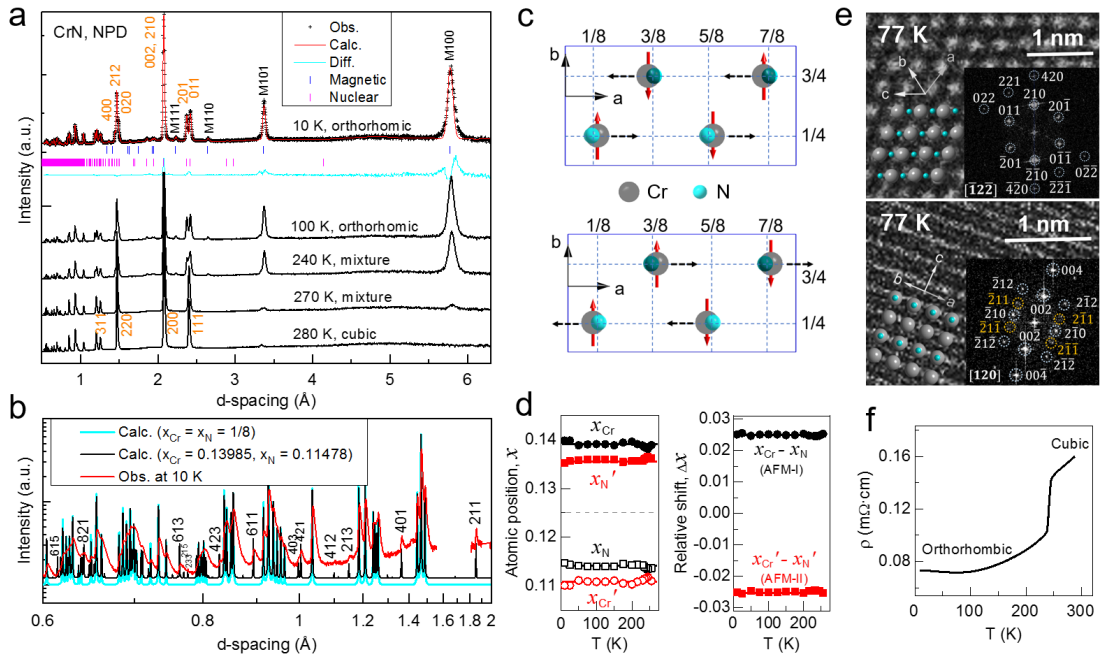

Fig. 1. Low-T neutron diffraction, resistivity, cryogenic TEM measurements. (**a**) Selected NPD patterns (90º bank). (**b**) High-resolution NPD pattern collected at 10 K (144º bank). Black and cyan lines represent the calculated using the nonpolar and polar structures, respectively. (**c**) Two equivalent structures of o-CrN: AFM-I and AFM-II. Red and black arrows denote the spin and atomic polarizations, respectively. (**d**) Refined x_{Cr} and x_N and their relative shift for both AFM-I and AFM-II. (**e**) Cryo-TEM images taken at 77 K. Insets are structure and electron diffraction patterns. (**f**) Low-T electrical resistivity measurement.

A paramagnetic (PM)-to-AFM phase transition starts at $T_N \approx 270$ K, coupled with a cubic (c)-to-orthorhombic (o) transition [Fig. 1(a)]. Using the reported *Pnma* structure as an initial model of o-CrN, atomic positions of Cr: 4c (x_{Cr}, 1/4, z_{Cr}) and N: 4c (x_N, 1/4, z_N) are accurately determined with x_{Cr} = 0.1398(5) and x_N = 0.1148(2) at 10 K

(Table S1). Note that the best refinement can only be achieved at fixed z_{Cr}= 1/4 and z_N = 3/4, indicating that *Pnma* may not be the most suitable structure. Instead, our symmetry analysis indicated that *Pmmn* with a higher symmetry is more favored. The refined magnetic structure has a P_anma symmetry, a maximal subgroup of *Pmmn* [Fig. 1(b) and Figs. S1-S4]. Table 1 summarizes the refined magnetic and nuclear lattice parameters for both phases; a 2×1×1 *Pmmn* super cell is used for properly describing both the nuclear and magnetic structures of o-CrN (Table S1). Both x_{Cr} and x_N deviate slightly from the ideal position of 1/8 and 5/8 (i.e., a nonpolar structure), resulting in a series of additional nuclear reflections (e.g., 211, 401, 213, 421, 611, 423, and 613). Such position deviations lead to a relative shift of positive and negative electric charges in opposite directions, producing local electric dipoles along the *a*-axis [Fig. 1(c)]. The resultant local polar sites 2*a* and 2*b* with a *mm2* symmetry belonging to a polar subgroup of *mmm* suggests an antiferroelectric-like transition [33] (Table 1). In fact, this long-range antiparallel ordering of dipoles formed by stacking of ferroelectric-like layers along the *b*-axis resembles that of traditional antiferroelectrics with similar centrosymmetric orthorhombic structures (e.g., $PbZrO_3$) [34]. Although the possible atomic distortion in o-CrN was previously evaluated [22], the nonpolar model is still the most frequently used and the structural ambiguity remains ignored. [23,26,35].

Magnetic refinement shows that o-CrN adopts an unusual AFM structure [Fig. 1(c)], as manifested by alternate stacking of double ferromagnetic sheets along the *a*-axis with a refined magnetic moment of 2.35(5) μ_B for Cr ions, close to previous reports [22,26].

According to the Goodenough-Kanamori Rules[36,37], this material is strongly AFM type, mainly due to the strong Cr-Cr magnetic interaction (Fig. S4). Interestingly, there exists an equivalent AFM phase with different spin orientations, leading to opposite shifts of atomic positions to x'_{Cr} = 0.1102(5) and 0.6102(5) and x'_{N} = 0.1352(2) and 0.6352(2) at 10 K. These two structural equivalents are denoted hereafter as AFM-I and AFM-II; they are mutually related by a mirror symmetry. Relative to their nonpolar positions of x = 1/8 and 5/8, both Cr and N atoms in the two structural equivalents have the same shifts of Δx_{Cr}= 0.014 and Δx_{N}= 0.011, respectively, and are nearly invariant at 10 - 270 K, showing a relative shift of Δx = 0.025 between Cr and N [Fig. 1(d)].

Table 1. Refined nuclear and magnetic structural parameters for CrN.

	Cubic (297 K)	Orthorhombic (10 K)	
		AFM-I	AFM-II
Symmetry	*Fm*$\bar{3}$*m* (No. 225)	*Pmmn* (No. 59)	*Pmmn* (No. 59)
a (Å)	4.1515 (5)	5.7693(1)	5.7693(1)
b (Å)	-	2.9711(1)	2.9711(1)
c (Å)	-	4.1413(1)	4.1413(1)
Cr	4a, (0, 0, 0)	2*a* (0.1398(5), 1/4, 1/4)	2*a* (0.1102(5), 1/4, 1/4)
		2*a* (0.6398(5), 1/4, 1/4)	2*a* (0.6102(5), 1/4, 1/4)
N	4b, (1/2, 1/2, 1/2)	2*b* (0.1148(2), 1/4, 3/4)	2*b* (0.1352(2), 1/4, 3/4)
		2*b* (0.6148(2), 1/4, 3/4)	2*b* (0.6352(2), 1/4, 3/4)
Moment (μ_B/Cr)	-	2.35(5)	2.35(5)
wR_P	3.1	1.6	1.6

The magnetic symmetry $P_a nma$ can be well described by a 2×1×1 *Pmmn* super cell with constrained coordinates: the two Cr: 2*a* and two N: 2*b* sites are fixed to be ½ along the a-axis (see Table S1).

The structural transition is confirmed by cryogenic transmission-electron microscopy (cryo-TEM) measurement; the electron diffraction pattern at 77 K can be indexed by o-CrN [Fig. 1(e)]. Along certain crystallographic directions (e.g., [120]), the extra peaks (e.g., 211) can be identified due to antiparallel atomic distortion. Besides, the intrinsic metallicity of both c- and o-CrN is determined by low-T resistivity

measurement [Fig. 1(f)]. A clear resistivity drop across T_N corresponds to the magnetostructural transition, and the measured resistivity is small and decreases with decreasing temperature for both phases, indicating their metallic behaviors [38,39].

To gain insights into the electronic structures of o-CrN, we calculated its band structure and projected density of states (DOS) [Figs. 2(a)-2(b)]. Note that the Hubbard potential U = 0.5 eV is an appropriate value for reproducing its magnetic moment, metallicity, and phonon instability (Figs. S5-S10). The deformed octahedral crystal field in o-CrN splits the Cr: 3d orbitals into t_{2g} and e_g states [Fig. 2(c)]. All three unpaired d-electrons tend to occupy t_{2g} orbitals below the Fermi level to form t_{2g}-t_{2g} band, indicative of spatially localized t_{2g} electrons. In o-CrN, their spins orientate to form an AFM order through a delicate competition between direct t_{2g}-t_{2g} AFM and ferromagnetic (FM) t_{2g}-N-t_{2g} exchange interactions [Figs. 2(a)-2(b) and Fig. S4].

The partially filled states around the Fermi level are predominated by the hybridization of Cr: e_g and N: p orbitals to form collectively shared states, which provide the only possible channel network for conducting electrons. The itinerant electrons could screen the Coulomb repulsion of t_{2g} electrons, leading to a small U for CrN, much smaller than that of ~3 eV for most insulating Cr-bearing compounds[40]. c-CrN also has similar partially filled states (i.e., metallic) (Fig. S7), confirming a metal-to-metal transition across T_N (Fig. 1). The decoupling of electronic transition from spin ordering would account for the coexistence of AFM and metallicity in CrN.

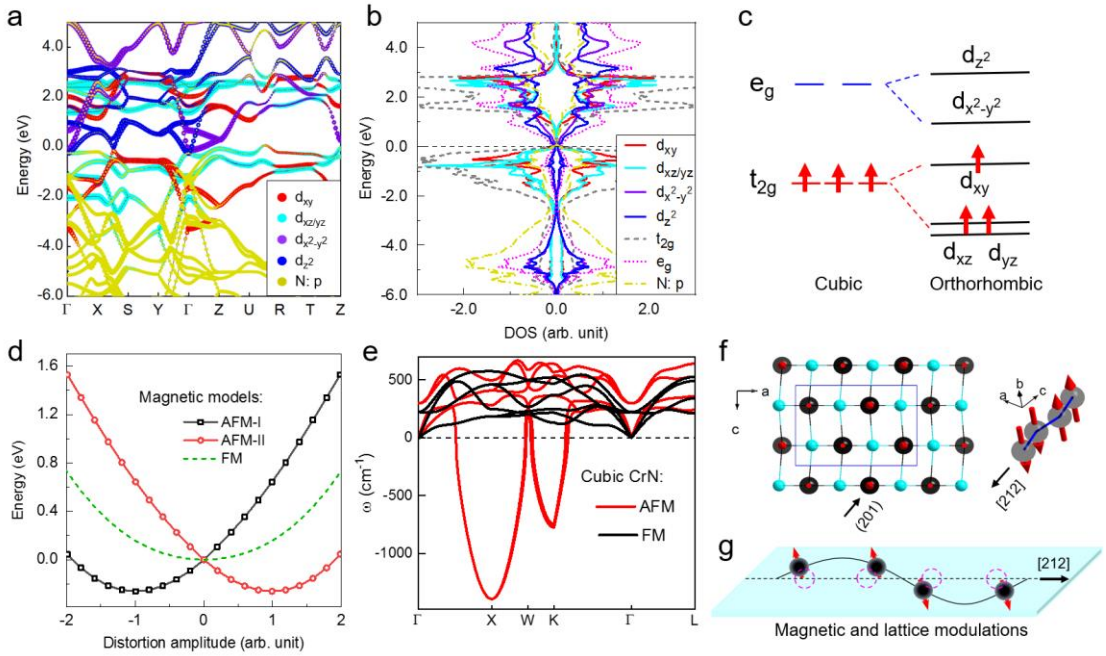

Fig. 2. Electronic structure, stability, and magnetostructural properties. (**a**) Band structure of o-CrN. The dots in different colors denote contributions from Cr: 3d and N: 2p states. (**b**) Projected DOS for o-CrN. (**c**) Spin states of CrN. (**d**) Potential energies vs. normalized antiparallel atomic distortion along the *a*-axis. (**e**) Phonon dispersions of c-CrN. (**f**) Structure of o-CrN and Ising-like spin chain. (**g**) Schematic diagram of lattice modulations by the frustrated spin chain of Cr atoms in o-CrN. The magenta circles denote collinearly aligned Cr atoms of the nonpolar phase.

In contrast to the FM model [Fig. 2(d)], calculations based on the AFM models reveal the bistability of CrN, as manifested by two single-well energy profiles with minimums located at atomic distortion amplitude of ±1, which explains the observed two equivalent AFM ground states [Fig. 1(c)]. With increasing distortion amplitude, a rapid decrease of energy penalty for both AFM models indicates the antiparallel atomic distortion is energetically favored. Evidently, both the spin and polar orderings in o-CrN originate from Cr atoms, which is the physical origin of coexisting polarity and magnetism in CrN.

Because of the spontaneous AFE-like transition in CrN, phonon instability of c-CrN should occur, as observed in traditional ferroelectrics [34]. We thus calculate the phonon dispersions for both phases using various magnetic models at selected U values and lattice parameters [Fig. 2(e) and Fig. S8]. Different from the situations in $PbZrO_3$ with soft transverse optical and acoustic branches [34,41,42], the structural instability in c-CrN is solely related to a soft phonon mode along the Γ-X line, resulting in antiparallel atomic displacements. Because a single unstable phonon mode cannot lead to antiferroelectric transition[34], other parameter is also at play. Spin ordering is the most possible factor that works cooperatively with soft structural mode for polar transition in CrN [Fig. 2(e)]. Our calculations show that the structural instability of c-CrN disappears in the FM model, suggesting a strong coupling of spin and polar orderings. A similar coupling in $BiFeO_3$ was recently recognized as electroacoustic magnon [43]. As expected, no phonon instability is observed in o-CrN (Fig. S8).

Origin of polar distortion in CrN can be elucidated from the ordering of spins and electric dipoles [Fig. 2(f)]. The buckling of Cr-N planes along the *c*-axis results in a relative shift of positive and negative charges of CrN_6 octahedra, leading to antiparallelly aligned electric dipoles. An Ising-like chain of frustrated spins occurs in the (201) plane with a large spin-frustration magnitude in comparable with that of $ZrCr_2O_4$ [44,45] (Fig. S4), which is the primary driving factor for producing antiparallel atomic distortions, resembling that of conventional improper ferroelectricity with a magnetic origin. Obviously, the nearest neighboring Cr atoms with antiparallel spins are pulled toward each other, whereas they mutually repel away when their spins are

parallel [Fig. 2(g)], which relieves frustration and leads to local polar distortion and dipole ordering [Fig. 1(c) and Figs. S3-S4].

The intriguing multiferroic-like transition in CrN can be understood within the framework of Landau theory [46]. With the allowed symmetry invariances, the energy E_O of low-symmetric o-CrN can be expanded in terms of distortions from high-symmetric c-CrN. Let X_5^- and mSM_3^+ denote the antiparallel atomic displacement and spin polarization at the X and SM points of the Brillouin zone, respectively [Fig. 3(a)]. Neglecting the homogeneous strains and high-order coupling terms, the energy of low-symmetric phase is given by

$$E_O = E_C + C_{20}Q_{X_5^-}^2 + C_{40}Q_{X_5^-}^4 + C_{60}Q_{X_5^-}^6 + C_{02}Q_{mSM_3^+}^2 + C_{04}Q_{mSM_3^+}^4 + C_{22}Q_{X_5^-}^2 \cdot Q_{mSM_3^+}^2 + C_{12}Q_{X_5^-} \cdot Q_{mSM_3^+}^2 \quad (1),$$

where $Q_{X_5^-}$ and $Q_{mSM_3^+}$ are the associated order parameters. The normalized atomic displacement and magnetic moment for o-CrN are $Q_{X_5^-} = \pm 1$ (i.e., relative shift $\Delta x \approx 0.025$) and $Q_{mSM_3^+} = 1$ (i.e., 2.33 μ_B), respectively, in contrast to those in non-magnetic c-CrN with $Q_{X_5^-} = Q_{mSM_3^+} = 0$. The last two terms $Q_{X_5^-}^2 \cdot Q_{mSM_3^+}^2$ and $Q_{X_5^-} \cdot Q_{mSM_3^+}^2$ correspond to magnetoelectric coupling. Constrained calculations give C_{20} (-0.315), C_{40} (0.111), C_{60} (0.027), C_{02} (-6.046), C_{04}(3.111), C_{22}(0.362) and C_{12}(-0.539) in a unit of eV. The negative C_{12} and positive C_{22} of the magnetoelectric coupling terms imply strong cooperative interaction and competition between the polar and spin orderings. This, combined with the fact that the magnetic P_anma symmetry is a subgroup of the nuclear *Pmmn*

symmetry, leads to a definitive conclusion that the magnetism plays a predominant role for the phase transition, according to the well-established symmetry criterion[47,48]. Our *ab initio* molecular dynamics simulations further reveal that the magnetism is indeed primary for initiating lattice instability in CrN (Fig. S10), consistent with previous reports[49,50]. However, because of the inadequacy of nonmagnetic calculations, a negative value is produced for the otherwise non-negative C_{20} (Fig. S10) that is related to the phonon instability at the X point. A wrinkled energy landscape is thus obtained for CrN with a minimum at $Q_{X_5^-} = Q_{mSM_3^+} = 1$ for AFM-I [Fig. 3(b)], and a degenerated state is located at $Q_{X_5^-} = -1$ and $Q_{mSM_3^+} = 1$ for AFM-II (Fig. S9). Clearly, the stability of o-CrN is dominant by the spin distortion, signaling an improper multiferroic-like transition. The linear coupling term $Q_{X_5^-}$ in Eq. 1 indicates a strong magnetoelectric effect, similar to that of magnetocaloric materials[51].

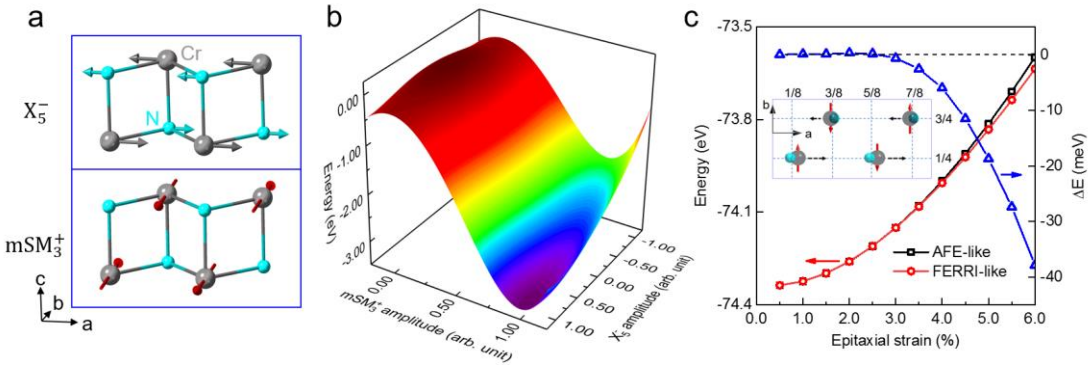

Fig. 3. Coupling of magnetic and polar orderings and calculations of strain-induced ferrielectric-like CrN. (**a**) AFE-like atomic displacements and AFM ordering associated with X_5^- and mSM_3^+ modes, respectively. (**b**) Calculated energy in terms of both X_5^- and mSM_3^+ amplitudes, using the AFM-I ordering (see Fig. S9 for that of AFM-II model and overall energy). The X_5^- amplitude corresponds to the normalized shift of Cr relative to N along the *a*-axis. (**c**) Energy comparison between FERRI- and AFE-like phases under tensile epitaxial strain with a difference of ΔE. Inset is a structure of FERRI-like phase (Fig. S11).

Considering the combined properties of metallicity, antiferroelectricity and antiferromagnetism in CrN, it is barely possible to manipulate its spin or charge by external fields. To make it technologically relevant, a net nonzero polarized CrN is a pre-requisite, which could be realized in epitaxially strained sample. Indeed, under epitaxial tensile strain in excess of 3%, our calculations show that the magnetostructural transition can spontaneously occur to form an energetically more favorable ferrielectric-like CrN [Fig. 3(c) and Fig. S11], while the metallicity is retained, making the control of its spins or charges by external fields possible. The metallicity disappears when the strain exceeds 5.0% with a metal-insulator transition.

Conclusions

In summary, CrN is identified as a rare metal that undergoes an improper multiferroic-like transition at low temperature. The polar order is linearly coupled and strongly driven by a frustrated antiferromagnetic spin ordering. Epitaxially strained o-CrN is also predicted to be a ferrielectric-like metal with tunable spin and charge. Coexistence of contra-indicated properties in CrN would provide a new platform for studies of diverse coupled phenomena (e.g., unconventional magnetoelectricity and complex spin-lattice coupling) and pave a way for designing unusual multiferroic-like metals by resorting to the magnetoelectric effect.

References:

[1] D. Khomskii, Physics **2**, 20 (2009).
[2] W. Eerenstein, N. D. Mathur, J. F. Scott, Nature **442**, 759 (2006).
[3] Y. Tokura, S. Seki, N. Nagaosa, Rep. Prog. Phys. **77**, 076501 (2014).
[4] S.-W. Cheong, M. Mostovoy, Nature Mater. **6**, 13 (2007).

[5] J. F. Scott, npj Comput. Mater. **1**, 15006 (2015).
[6] Y. Shi, Y. Guo, X. Wang, A. J. Princep, D. Khalyavin, P. Manuel, Y. Michiue, A. Sato, K. Tsuda, S. Yu, M. Arai, Y. Shirako, M. Akaogi, N. Wang, K. Yamaura, A. T. Boothroyd, Nature Mater. **12**, 1024 (2013).
[7] P. W. Anderson, E. I. Blount, Phys. Rev. Lett. **14**, 217 (1965).
[8] N. A. Benedek, T. Birol, J. Mater. Chem. C **4**, 4000 (2016).
[9] H. Fu, Phys. Rev. B **102**, 134118 (2020).
[10] D. Puggioni, J. M. Rondinelli, Nature Commun. **5**, 3432 (2014).
[11] J. Lu, G. Chen, W. Luo, J. Íñiguez, L. Bellaiche, H. Xiang, Phys. Rev. Lett. **122**, 227601 (2019).
[12] J. J. Gao, S. Y. Fu, K. Yamaura, J. F. Lin, J. S. Zhou, Phys. Rev. B **101**, 220101 (2020).
[13] Z. Fei, W. Zhao, T. A. Palomaki, B. Sun, M. K. Miller, Z. Zhao, J. Yan, X. Xu, D. H. Cobden, Nature **560**, 336 (2018).
[14] H. Sakai, K. Ikeura, M. S. Bahramy, N. Ogawa, D. Hashizume, J. Fujioka, Y. Tokura, S. Ishiwata, Sc. Adv. **2**, e1601378 (2016).
[15] T. H. Kim, D. Puggioni, Y. Yuan, L. Xie, H. Zhou, N. Campbell, P. J. Ryan, Y. Choi, J. W. Kim, J. R. Patzner, S. Ryu, J. P. Podkaminer, J. Irwin, Y. Ma, C. J. Fennie, M. S. Rzchowski, X. Q. Pan, V. Gopalan, J. M. Rondinelli, C. B. Eom, Nature **533**, 68 (2016).
[16] N. J. Laurita, A. Ron, J.-Y. Shan, D. Puggioni, N. Z. Koocher, K. Yamaura, Y. Shi, J. M. Rondinelli, D. Hsieh, Nature Commun. **10**, 3217 (2019).
[17] W. Cai, J. He, H. Li, R. Zhang, D. Zhang, D. Y. Chung, T. Bhowmick, C. Wolverton, M. G. Kanatzidis, S. Deemyad, Nature Commun. **12**, 1509 (2021).
[18] A. Filippetti, V. Fiorentini, F. Ricci, P. Delugas, J. Íñiguez, Nature Commun. **7**, 11211 (2016).
[19] I. Marković, M. D. Watson, O. J. Clark, F. Mazzola, E. Abarca Morales, C. A. Hooley, H. Rosner, C. M. Polley, T. Balasubramanian, S. Mukherjee, N. Kikugawa, D. A. Sokolov, A. P. Mackenzie, P. D. C. King, Proc. Nat. Acad. Sci. USA **117**, 15524 (2020).
[20] A. J. Princep, H. L. Feng, Y. F. Guo, F. Lang, H. M. Weng, P. Manuel, D. Khalyavin, A. Senyshyn, M. C. Rahn, Y. H. Yuan, Y. Matsushita, S. J. Blundell, K. Yamaura, A. T. Boothroyd, Phys. Rev. B **102**, 104410 (2020).
[21] H. L. Feng, C.-J. Kang, P. Manuel, F. Orlandi, Y. Su, J. Chen, Y. Tsujimoto, J. Hadermann, G. Kotliar, K. Yamaura, E. E. McCabe, M. Greenblatt, Chem. Mater. **33**, 4188 (2021).
[22] L. M. Corliss, N. Elliott, J. M. Hastings, Phys. Rev. **117**, 929 (1960).
[23] F. Rivadulla, M. Banobre-Lopez, C. X. Quintela, A. Pineiro, V. Pardo, D. Baldomir, M. A. Lopez-Quintela, J. Rivas, C. A. Ramos, H. Salva, J. S. Zhou, J. B. Goodenough, Nature Mater. **8**, 947 (2009).
[24] P. A. Bhobe, A. Chainani, M. Taguchi, T. Takeuchi, R. Eguchi, M. Matsunami, K. Ishizaka, Y. Takata, M. Oura, Y. Senba, H. Ohashi, Y. Nishino, M. Yabashi, K. Tamasaku, T. Ishikawa, K. Takenaka, H. Takagi, S. Shin, Phys. Rev. Lett. **104**, 236404 (2010).
[25] Y. Tsuchiya, K. Kosuge, Y. Ikeda, T. Shigematsu, S. Yamaguchi, N. Nakayama, Mater. Trans., JIM **37**, 121 (1996).
[26] A. Filippetti, N. A. Hill, Phys. Rev. Lett. **85**, 5166 (2000).
[27] S. Wang, X. Yu, J. Zhang, M. Chen, J. Zhu, L. Wang, D. He, Z. Lin, R. Zhang, K. Leinenweber, Y. Zhao, Phys. Rev. B **86**, 064111 (2012).
[28] B. Alling, T. Marten, I. A. Abrikosov, Nature Mater. **9**, 283 (2010).
[29] S. Wang, X. Yu, J. Zhang, L. Wang, K. Leinenweber, D. He, Y. Zhao, Cryst. Growth Des. **16**, 351 (2016).

[30] M. Chen, S. Wang, J. Zhang, D. He, Y. Zhao, Chem. Eur. J. **18**, 15459 (2012).
[31] S. C. Vogel, C. Hartig, L. Lutterotti, R. B. Von Dreele, H.-R. Wenk, D. J. Williams, Powder Diffr. **19**, 65 (2004).
[32] See Supplemental Material at http://link.aps.org/supplemental/10.xxxxx for experimental methods and more details of neutron diffraction refinements, nuclear and magnetic symmetry analysis, calculations of band structures and phonon dispersions, molecular dynamics simulations of spin-lattice coupling, and so on.
[33] P. Tolédano, M. Guennou, Phys. Rev. B **94**, 014107 (2016).
[34] A. K. Tagantsev, K. Vaideeswaran, S. B. Vakhrushev, A. V. Filimonov, R. G. Burkovsky, A. Shaganov, D. Andronikova, A. I. Rudskoy, A. Q. R. Baron, H. Uchiyama, D. Chernyshov, A. Bosak, Z. Ujma, K. Roleder, A. Majchrowski, J. H. Ko, N. Setter, Nature Commun. **4**, 2229 (2013).
[35] A. Filippetti, W. E. Pickett, B. M. Klein, Phys. Rev. B **59**, 7043 (1999).
[36] J. Kanamori, J. Phys. Chem. Solids **10**, 87 (1959).
[37] J. B. Goodenough, J. Phys. Chem. Solids **6**, 287 (1958).
[38] C. X. Quintela, J. P. Podkaminer, M. N. Luckyanova, T. R. Paudel, E. L. Thies, D. A. Hillsberry, D. A. Tenne, E. Y. Tsymbal, G. Chen, C.-B. Eom, F. Rivadulla, Adv. Mater. **27**, 3032 (2015).
[39] Q. Jin, H. Cheng, Z. Wang, Q. Zhang, S. Lin, M. A. Roldan, J. Zhao, J.-O. Wang, S. Chen, M. He, C. Ge, C. Wang, H.-B. Lu, H. Guo, L. Gu, X. Tong, T. Zhu, S. Wang, H. Yang, K.-j. Jin, E.-J. Guo, Adv. Mater. **33**, 2005920 (2021).
[40] M. Imada, A. Fujimori, Y. Tokura, Rev. Mod. Phys. **70**, 1039 (1998).
[41] D. Viehland, Phys. Rev. B **52**, 778 (1995).
[42] P. Ghosez, E. Cockayne, U. V. Waghmare, K. M. Rabe, Phys. Rev. B **60**, 836 (1999).
[43] S. O. Sayedaghaee, B. Xu, S. Prosandeev, C. Paillard, L. Bellaiche, Phys. Rev. Lett. **122**, 097601 (2019).
[44] A. P. Ramirez, Annu. Rev. Mater. Sci. **24**, 453 (1994).
[45] S. H. Lee, C. Broholm, T. H. Kim, W. Ratcliff, S. W. Cheong, Phys. Rev. Lett. **84**, 3718 (2000).
[46] M. Reis, in *Fundamentals of Magnetism*, edited by M. Reis (Academic Press, Boston, 2013), pp. 177.
[47] D. M. Hatch, H. T. Stokes, Phase Transit. **7**, 087 (1986).
[48] D. M. Hatch, H. T. Stokes, Phys. Rev. B **65**, 014113 (2001).
[49] A. Lindmaa, R. Lizárraga, E. Holmström, I. A. Abrikosov, B. Alling, Phys. Rev. B **88**, 054414 (2013).
[50] I. Stockem, A. Bergman, A. Glensk, T. Hickel, F. Körmann, B. Grabowski, J. Neugebauer, B. Alling, Phys. Rev. Lett. **121**, 125902 (2018).
[51] E. K. H. Salje, M. A. Carpenter, J. Phys. Condens. Matter **23**, 462202 (2011).

Acknowledgments

This work was supported by the National Natural Science Foundation of China (Grant No. 12174175), the Guangdong Innovative & Entrepreneurial Research Team Program (No. 2016ZT06C279), the Shenzhen Peacock Plan (No. KQTD2016053019134356), and the Shenzhen Development and Reform Commission Foundation for Shenzhen Engineering Research Center for Frontier Materials Synthesis at High Pressure. This work was also partially funded by the National Natural Science Foundation of China under Grant No. 11774142, Grant No. 11974390 and Grant No. 12004160, and the Shenzhen Basic

Research Fund under Grant No. JCYJ20180504165817769 and Grant No. JCYJ20190809173213150. The computer time was supported by the Center for Computational Science and Engineering of SUSTech. The use of cryogenic TEM was supported by the Cryo-TEM Center of SUSTech. This work has partly benefited from the use of the HiPPO beamline of LANSCE at LANL, which was formerly funded by the U.S. DOS-BES. L.B. thanks the Vannevar Bush Faculty Fellowship (VBFF) from the Department of Defense. X. Yu acknowledges the research fund for supporting the Synergic Extreme Condition User Facility (SECUF) at Beijing.

Competing interests

The authors declare no competing interests.

Author information

§ These authors contributed equally to this work.

*E-mail: huangl@sustech.edu.cn (L. Huang); wangsm@sustech.edu.cn (S. Wang)